GEOPHYSICS, VOL. 63, NO. 6 (NOVEMBER-DECEMBER 1998); P. 1898–1907, 5 FIGS.

Magnetotelluric tensor decomposition: Part II, Examples of a basic procedure

F. E. M. (Ted) Lilley*

ABSTRACT

The decomposition procedure suggested for magnetotelluric (MT) data in a companion paper is illustrated by examples. Adjacent pairs of stations are examined to test for common features in their MT response. The method analyzes the real and quadrature parts of an impedance tensor separately, and the results for the real and quadrature parts are compared, and in some cases combined, at the end. Values are obtained which are interpreted directly in terms of nearest 2-D principal impedances, local geologic strike, and regional geologic strike.

The requirement for valid data derived in the companion paper, that $Z_{xy_r} Z_{yx_r} < Z_{xx_r} Z_{yy_r}$ together with $Z_{xy_q} Z_{yx_q} < Z_{xx_q} Z_{yy_q}$, is shown to be a useful criterion in the winnowing of erroneous data.

The examples presented typically show the direction interpreted as local geologic strike to be well determined, period independent, and consistent between real and quadrature MT matrices. In these examples, however, the direction interpreted as regional geologic strike is period dependent and not in good agreement between real and quadrature MT matrices. These results suggest caution is desirable in the use of period-independent galvanic distortion models, which should be checked first with regional strike determinations.

INTRODUCTION

In this paper a decomposition method for magnetotelluric (MT) data, which is derived in a companion paper (Lilley, 1998), is illustrated with four worked examples. The examples presented are intentionally ones based on case histories already established in the literature; the unrotated MT tensor data were made available for the First Magnetotelluric Data Interpretation Workshop (held in Wellington, New Zealand, in 1992) to compare data processing and interpretation methods. It is often the case that the better known such example data sets become and the more thoroughly they are examined by different methods, the more valuable they are to the development of their discipline.

Though the data have been analyzed by others, the present method is different, and the results are new. The procedure analyzes an MT tensor in terms of its real and quadrature matrices taken separately. From the four values which comprise one such matrix, four other values are derived which are interpreted as estimates of major and minor impedance, local strike, and regional strike. Real and quadrature results are combined to give complex major and minor impedance values, and the method allows the real and quadrature parts of a tensor to have different skew values. The values interpreted as the local and regional strikes give the skew values directly.

The examples show that it is common for actual data to give a well-determined local strike, but no more than poor indications of a regional strike. Real and quadrature "principal values", however, are given by the present decomposition method directly and are not dependent on the determination of a period-independent regional strike. These real and quadrature principal values represent the closest 2-D models, in a clearly defined sense, to the real and quadrature matrices of the tensor examined separately; they may be combined to give "principal impedance" values, again in a clearly defined sense.

The following notation is adopted in this paper: $\mathbf{Z}$ (of elements Z_{xx}, Z_{xy}, Z_{yx}, Z_{yy}) denotes the MT impedance tensor with axes in the orientation of field observation (aligned north and east). $\mathbf{Z}'$ (of elements Z'_{xx}, Z'_{xy}, Z'_{yx}, Z'_{yy}) denotes the impedance tensor after axis rotation.

There is commonly an ambiguity of 90° in the determinations of strike direction in this paper. The ambiguity arises because when axes are rotated to achieve an ideal 2-D form for a tensor, there is no indication from the MT data alone which axis direction is along strike and which is across strike. Strike direction thus has a 90° ambiguity.

Manuscript received by the Editor June 9, 1997; revised manuscript received May 14, 1998.
*Research School of Earth Sciences, Australian National University, Canberra, A.C.T 0200, Australia. E-mail: Ted.Lilley@anu.edu.au.

DESCRIPTION OF DATA

Four examples are given in which the formulas of the companion paper (Lilley, 1998) are applied to observed tensors. A particular value of these examples is that the tensors examined are already in the literature as worked examples, and the new decomposition results presented here may be compared to others published earlier.

The examples are from sites LIT000, LIT001, LIT007, and LIT008 of the BC87 dataset (Jones et al., 1988; Jones, 1993; see also Groom et al., 1993, and Chave and Jones, 1997), which formed the basis for analysis, interpretation, and discussion at the First Magnetotelluric Data Interpretation Workshop (MT-DIW1), held in Wellington, New Zealand, in 1992 (Ingham et al., 1993). The examples have intentionally been chosen as pairs of adjacent sites, and are presented and discussed in this way. Adjacent sites may be expected to show some common features because they share the same regional setting.

In the companion paper (Lilley, 1998), a data criterion was described based on the requirement that a regular MT Mohr circle should not include the origin of the axes (this was shown to reduce to the requirement that $Z_{xy_r} Z_{yx_r} < Z_{xx_r} Z_{yy_r}$ together with $Z_{xy_q} Z_{yx_q} < Z_{xx_q} Z_{yy_q}$). This criterion has been applied in the examples analyzed in this paper. For data failing the criterion, no minor principal impedance (Z^P_{xy}) results are obtained; instead, the apparent resistivity and phase values for Z^P_{xy} are arbitrarily set at 25 000 ohm-m and 165°, respectively, to enable their clear identification on plots of the decomposition parameters.

FORMULAS FOR DECOMPOSITION

The key equations from the companion paper (Lilley, 1998) are first stated, with subscript r for real and q for quadrature.

The observed tensor is

$$\begin{bmatrix} Z_{xx_r} + i Z_{xx_q} & Z_{xy_r} + i Z_{xy_q} \\ Z_{yx_r} + i Z_{yx_q} & Z_{yy_r} + i Z_{yy_q} \end{bmatrix}. \tag{1}$$

The twist is

$$\gamma_r = \arctan\left[\frac{Z_{yy_r} + Z_{xx_r}}{Z_{xy_r} - Z_{yx_r}}\right], \tag{2}$$

$$\gamma_q = \arctan\left[\frac{Z_{yy_q} + Z_{xx_q}}{Z_{xy_q} - Z_{yx_q}}\right], \tag{3}$$

and the criterion that the circumference of a circle should not enclose its origin of axes is

$$Z_{xy_r} Z_{yx_r} < Z_{xx_r} Z_{yy_r}, \tag{4}$$

$$Z_{xy_q} Z_{yx_q} < Z_{xx_q} Z_{yy_q}. \tag{5}$$

The principal values are

$$Z^P_{xy_r} = \tfrac{1}{2}\Big\{\big[\big(Z_{yy_r} + Z_{xx_r}\big)^2 + \big(Z_{yx_r} - Z_{xy_r}\big)^2\big]^{\frac{1}{2}} - \big[\big(Z_{yy_r} - Z_{xx_r}\big)^2 + \big(Z_{xy_r} + Z_{yx_r}\big)^2\big]^{\frac{1}{2}}\Big\}, \tag{6}$$

$$Z^P_{xy_q} = \tfrac{1}{2}\Big\{\big[\big(Z_{yy_q} + Z_{xx_q}\big)^2 + \big(Z_{yx_q} - Z_{xy_q}\big)^2\big]^{\frac{1}{2}} - \big[\big(Z_{yy_q} - Z_{xx_q}\big)^2 + \big(Z_{xy_q} + Z_{yx_q}\big)^2\big]^{\frac{1}{2}}\Big\}, \tag{7}$$

and

$$Z^P_{yx_r} = \tfrac{1}{2}\Big\{\big[\big(Z_{yy_r} + Z_{xx_r}\big)^2 + \big(Z_{yx_r} - Z_{xy_r}\big)^2\big]^{\frac{1}{2}} + \big[\big(Z_{yy_r} - Z_{xx_r}\big)^2 + \big(Z_{xy_r} + Z_{yx_r}\big)^2\big]^{\frac{1}{2}}\Big\}, \tag{8}$$

$$Z^P_{yx_q} = \tfrac{1}{2}\Big\{\big[\big(Z_{yy_q} + Z_{xx_q}\big)^2 + \big(Z_{yx_q} - Z_{xy_q}\big)^2\big]^{\frac{1}{2}} + \big[\big(Z_{yy_q} - Z_{xx_q}\big)^2 + \big(Z_{xy_q} + Z_{yx_q}\big)^2\big]^{\frac{1}{2}}\Big\}. \tag{9}$$

The direction of E-axis strike, reasonably interpreted as the direction of local geologic strike, is

$$\theta_{e_r} = \frac{1}{2}\left[\arctan\frac{Z_{yy_r} - Z_{xx_r}}{Z_{xy_r} + Z_{yx_r}} + \arctan\frac{Z_{yy_r} + Z_{xx_r}}{Z_{xy_r} - Z_{yx_r}}\right], \tag{10}$$

$$\theta_{e_q} = \frac{1}{2}\left[\arctan\frac{Z_{yy_q} - Z_{xx_q}}{Z_{xy_q} + Z_{yx_q}} + \arctan\frac{Z_{yy_q} + Z_{xx_q}}{Z_{xy_q} - Z_{yx_q}}\right]. \tag{11}$$

The direction of H-axis strike, possibly interpreted as the direction of regional geologic strike, is

$$\theta_{h_r} = \frac{1}{2}\left[\arctan\frac{Z_{yy_r} - Z_{xx_r}}{Z_{xy_r} + Z_{yx_r}} - \arctan\frac{Z_{yy_r} + Z_{xx_r}}{Z_{xy_r} - Z_{yx_r}}\right], \tag{12}$$

$$\theta_{h_q} = \frac{1}{2}\left[\arctan\frac{Z_{yy_q} - Z_{xx_q}}{Z_{xy_q} + Z_{yx_q}} - \arctan\frac{Z_{yy_q} + Z_{xx_q}}{Z_{xy_q} - Z_{yx_q}}\right]. \tag{13}$$

The angles θ_e and θ_h are measured clockwise from the axes (taken to be orthogonal) which were used for the field observation of the magnetotelluric data.

The above equations illustrate how the "two-mode" convention applies, so that the given quantities may be computed on a period-by-period basis for both real and quadrature modes. For angles, the real and quadrature mode values may then be averaged. For the principal impedances, the real and quadrature principal values may be combined to give complex impedance values. Forming a complex impedance value in this way carries the implication of recognizing that the real and quadrature parts of a tensor may have different values of θ_e, θ_h, and twist.

SITES LIT000 AND LIT001

Summaries of the complete MT tensor data for sites LIT000 and LIT001 are shown in Figure 1. For each site, the upper four pairs of graphs on the left side show the raw (as distributed for

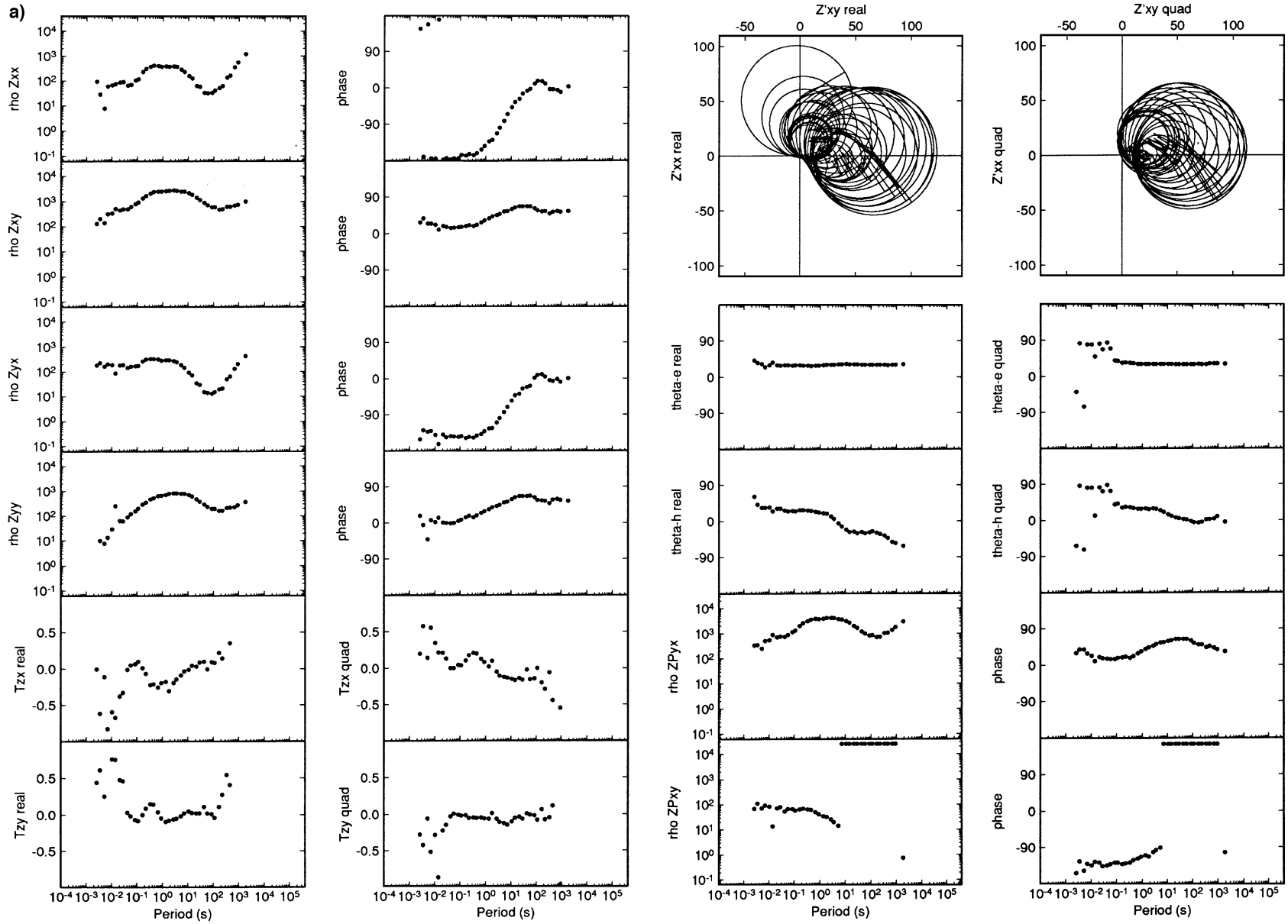

FIG. 1. Complete data for sites LIT000 (a) and LIT001 (b). Units of apparent resistivity are ohm-m. Angles are given in degrees.

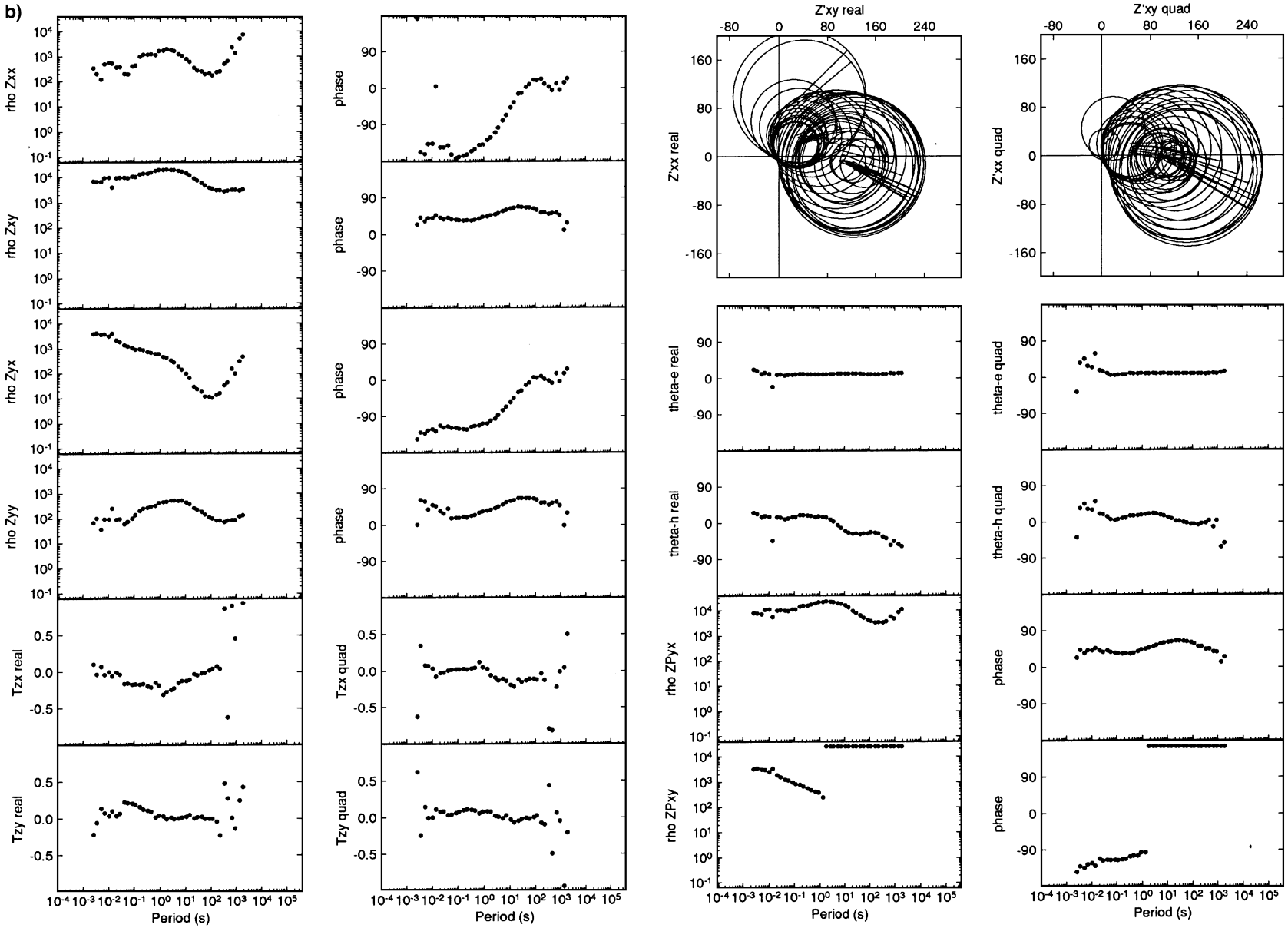

FIG. 1. (Continued.)

the workshop) tensor element data, presented as amplitude and phase values; thus "rho Zxy" is the apparent resistivity given by the Z_{xy} complex impedance tensor element. The lower two graphs on the left side show the vertical field transfer functions T_{zx} and T_{zy}, included for completeness.

On the right side of each figure are, first, Mohr diagrams for the observed tensor (type 1 as in Figure 2 of Lilley, 1998), plotted with impedance element values normalized by multiplication by $\mathcal{T}^{1/2}$, where $\mathcal{T}$ denotes period. This normalization allows for the general decrease of such tensor elements with increasing period (according to $\mathcal{T}^{-1/2}$ for a uniform half-space).

Below these diagrams are the decomposition parameters determined by equations (6) to (13). The angles θ_e and θ_h, real and quadrature, are plotted as functions of period, and principal impedances are presented as apparent resistivity and phase values. The principal impedance values result from combining real and quadrature principal values which have been determined separately. Principal impedance values, formed in this way, allow the real and quadrature parts of a tensor to have different values for θ_e, θ_h, and twist.

Sites LIT000 and LIT001 are some 10 km apart. The similarities in their raw data are made more orderly in the decomposition parameters. A major difference between them is the increase, by perhaps an order of magnitude, in the apparent resistivity for Z^P_{yx}, the major principal impedance, of LIT001 relative to LIT000. This difference may correspond to the position of LIT001 on the Nelson Batholith, whereas LIT000 is east of this major geological structure.

For both LIT000 and LIT001, the θ_e values from the decomposition are very constant over the whole period range, with real values agreeing with quadrature. Local geologic strike directions for the two sites are thus clearly indicated, (30° for LIT000, and 10° for LIT001). The θ_h values are seen to be period dependent, with poor agreement between real and quadrature for each station, so that the case for a period-independent regional strike is not clear for these data. However, the θ_h values, taking real and quadrature separately, are in good agreement between the two sites, which will be discussed further below.

Otherwise, it can be seen that the decomposition has produced principal impedances which are well behaved in phase. Many data of period greater than 1 s have been found invalid for use in determining minor principal impedance values, using the criterion that both $Z_{xy_r} Z_{yx_r} < Z_{xx_r} Z_{yy_r}$ and $Z_{xy_q} Z_{yx_q} < Z_{xx_q} Z_{yy_q}$ should be satisfied for valid data. The occurrence of the invalid data is attributed to the high anisotropy of the raw tensor data, combined with the data errors. The high anisotropy of the raw data has meant that the minor principal impedance values are sufficiently low, that errors have made these particular ones indistinguishable from zero, with phase values which are indeterminate.

Figure 2 shows, plotted together, just the decomposition parameters for LIT000 and LIT001. Some of the characteristics seen in Figure 1 are now clearer, especially the remarkable agreement in the corresponding θ_h values for the two sites, and in the phases for the principal impedances.

SITES LIT007 AND LIT008

Summaries of the complete MT tensor data for sites LIT007 and LIT008 are shown in Figure 3. Sites LIT007 and LIT008 are about 1 km apart, and so would be expected to show very similar characteristics. However, as already remarked upon by Jones (1993) and Jones and Groom (1993), the raw data for LIT008 (left side of Figure 3b) appear quite well behaved, whereas the raw data for LIT007 (left side of Figure 3a) show some phase values out of their expected quadrant.

The decomposition parameters for the two sites, shown on the right halves of Figures 3a and 3b, appear to resolve the differences in the raw data. Again the θ_e values are constant with period, in agreement between real and quadrature data, and in close agreement between the two sites (the values are −70° for LIT007 and −65° for LIT008). The principal impedances are also in good agreement between the two sites, as shown by the apparent resistivity curves.

The θ_h results, however, are distinctive and explain the differences in the raw data. For neither site is a period-independent regional strike indicated by the θ_h data, and again there is only poor agreement between real and quadrature θ_h values at each site. In both real and quadrature graphs, however, the LIT007 values can be seen to have an "antisymmetry" to the LIT008 values. This characteristic is in strong contrast to the LIT000-LIT001 case, where the θ_h values were in close agreement between sites.

Figure 4 shows, plotted together, just the decomposition parameters for LIT007 and LIT008. The figure emphasizes the constancy and agreement in the θ_e values, the antisymmetry in the θ_h values, and the agreement in the principal impedances (both apparent resistivity and phase).

GENERAL COMMENTS

All four examples show θ_e remarkably independent of period, and consistent between real and quadrature. [It is important to note that this direction is not the preferred direction of electric field evident from a simple plot of the elements of an impedance tensor. In the top part Figure 2 of the companion paper (Lilley, 1998), that direction is given by rotation of the radial arm by β clockwise from the observed point, rather than by ϕ_1 counterclockwise.]

Also, in the four cases examined here, θ_h varies with period. Typically θ_h is close to θ_e at short periods, but it twists away as period lengthens, with only approximate similarity between real and quadrature values for a given station. For LIT000 and LIT001, the pairs of θ_h functions are very similar between the two stations; whereas LIT007 and LIT008 provide a case history of stations close together, where the θ_h functions show an antisymmetry.

Clearly, among the decomposition parameters, the $(\theta_e - \theta_h)$ parameter is the major indicator of three dimensionality. The present examples do not display strong evidence of a regional geological strike different from the local strike; however, if period-dependent "twisting" of the H-axes relative to the E-axes is accepted, then the principal impedances are determined independent of the question of regional geologic strike. Particularly, the agreement shown in Figure 4 for the principal impedance apparent resistivities and phases between LIT007 and LIT008 supports this point. If a 2-D interpretation is to be made of a situation such as shown in Figure 4, the principal impedances to be matched by a 2-D model may be the most important parameters to determine.

CONCLUSIONS

Actual examples decomposed by the analysis of the companion paper (Lilley, 1998) typically show rotated E-axes directions constant with period and between real and quadrature modes, convincingly indicating the existence of a local geologic strike and its measurement. These examples, however, do not strongly support the concept of a period-independent regional strike, indicated by H axes which are twisted away from alignment with the E axes by a period-independent twist. Rather, the twist angle is typically zero at high frequency, with no indication of a regional strike different from the local strike. Only at long periods may the H axes move away ("twist away") from the E axes.

It may also be appropriate to note here that a benefit of the Mohr diagram construction for MT data is that it provides a clear way of checking, when an MT tensor is being rotated, that both conceptually and numerically the rotation is being carried out correctly. Experience on several occasions has shown such diagrams detecting errors. Appendix A describes a procedure for initially sketching Mohr diagrams for known data.

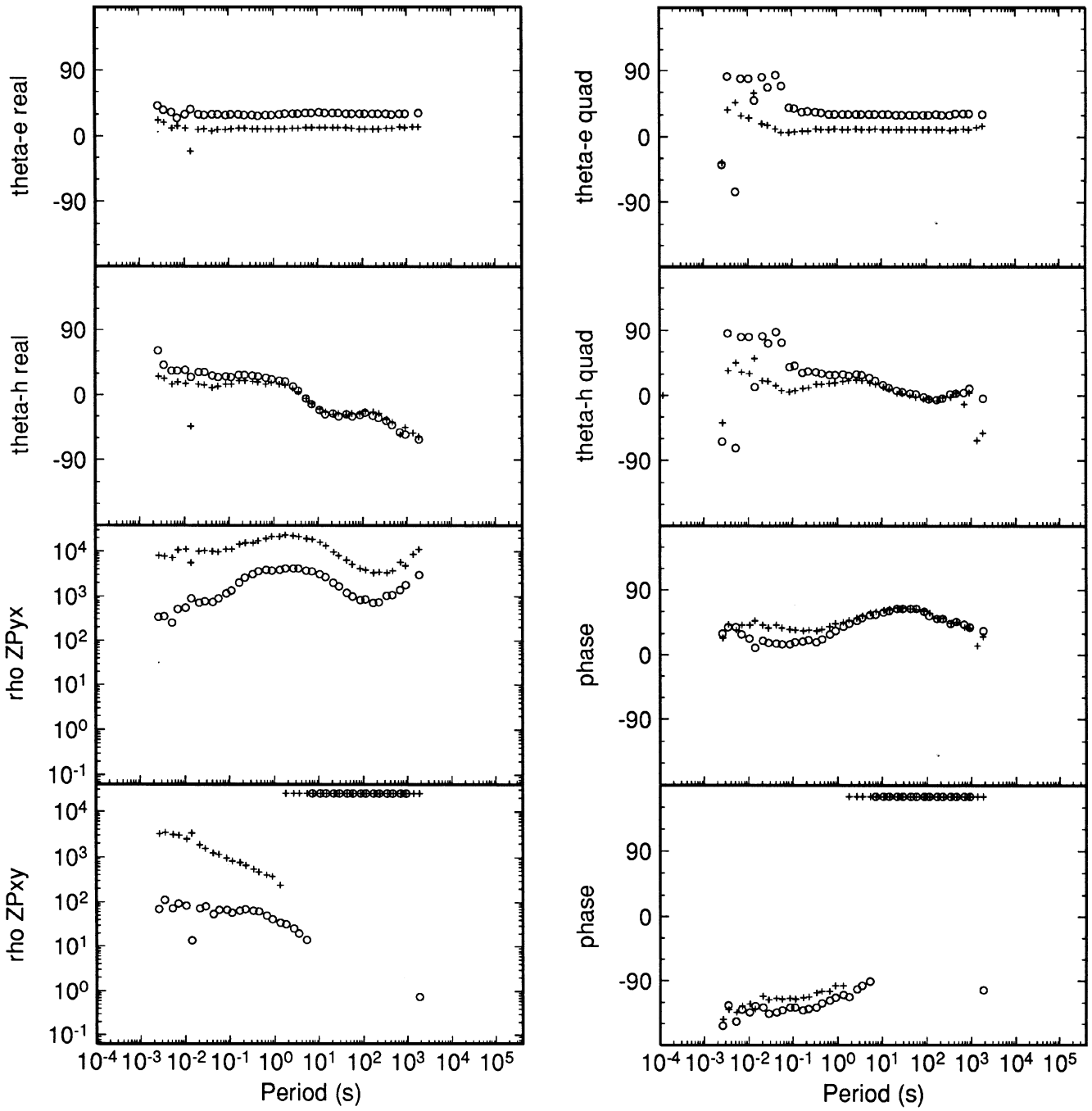

FIG. 2. Superimposed plots for decomposition parameters of LIT000 (circles) and LIT001 (crosses). The scatter of points in the quadrature θ_e and θ_h values for LIT000 at short periods is due to the data being 1-D (and so θ_e and θ_h are undefined).

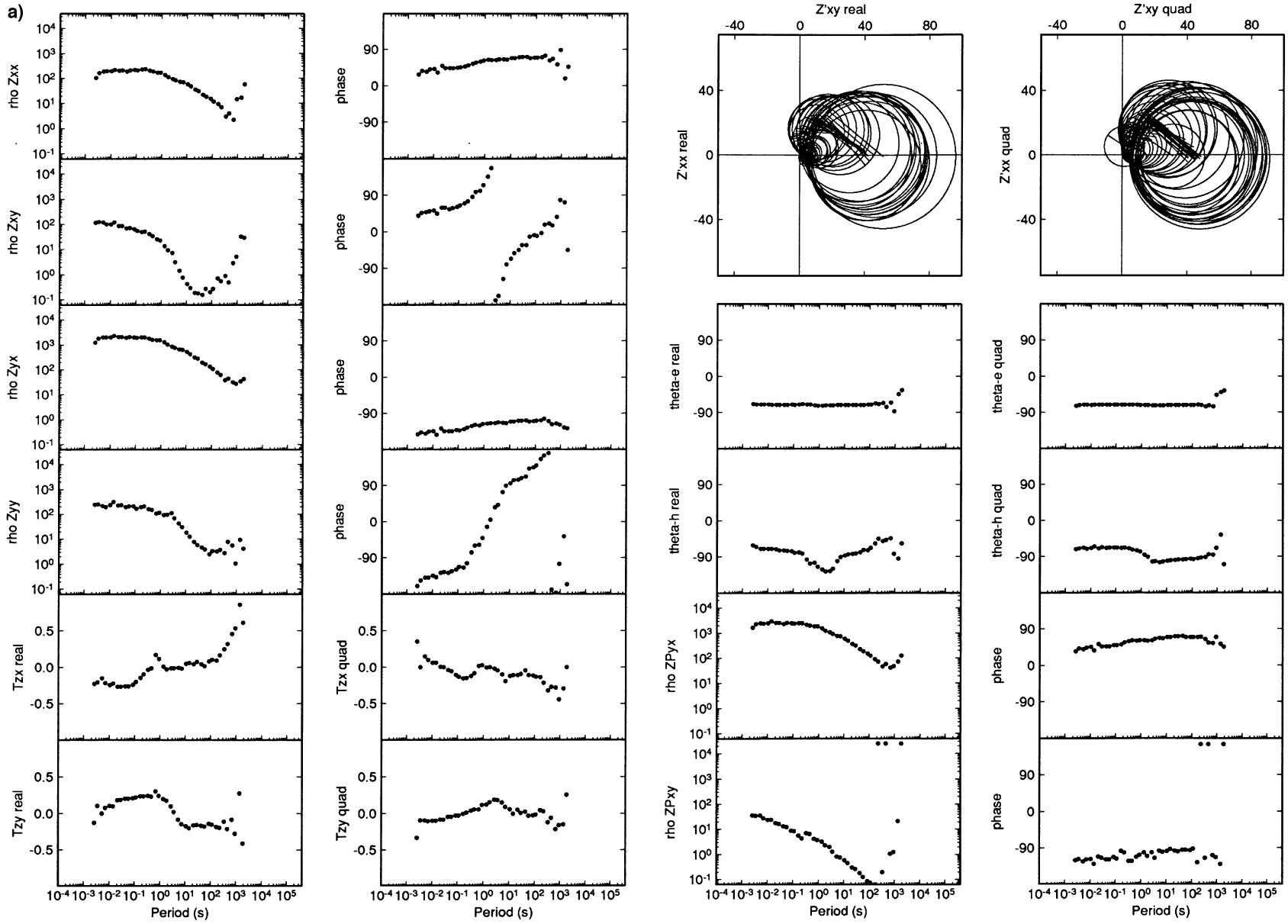

FIG. 3. Complete data for LIT007 (a) and LIT008 (b). Units of apparent resistivity are ohm-m. Angles are given in degrees.

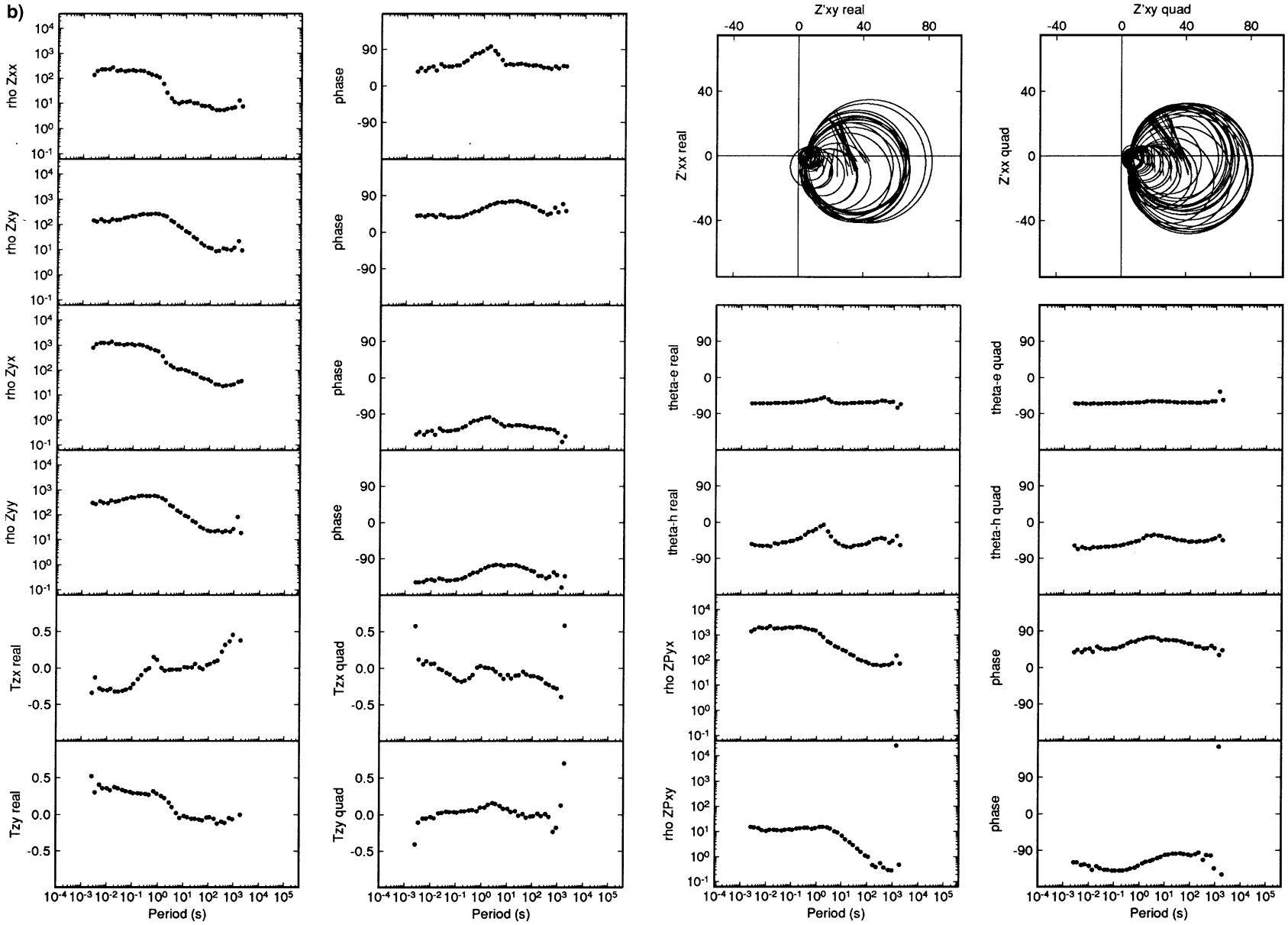

FIG. 3. (Continued.)

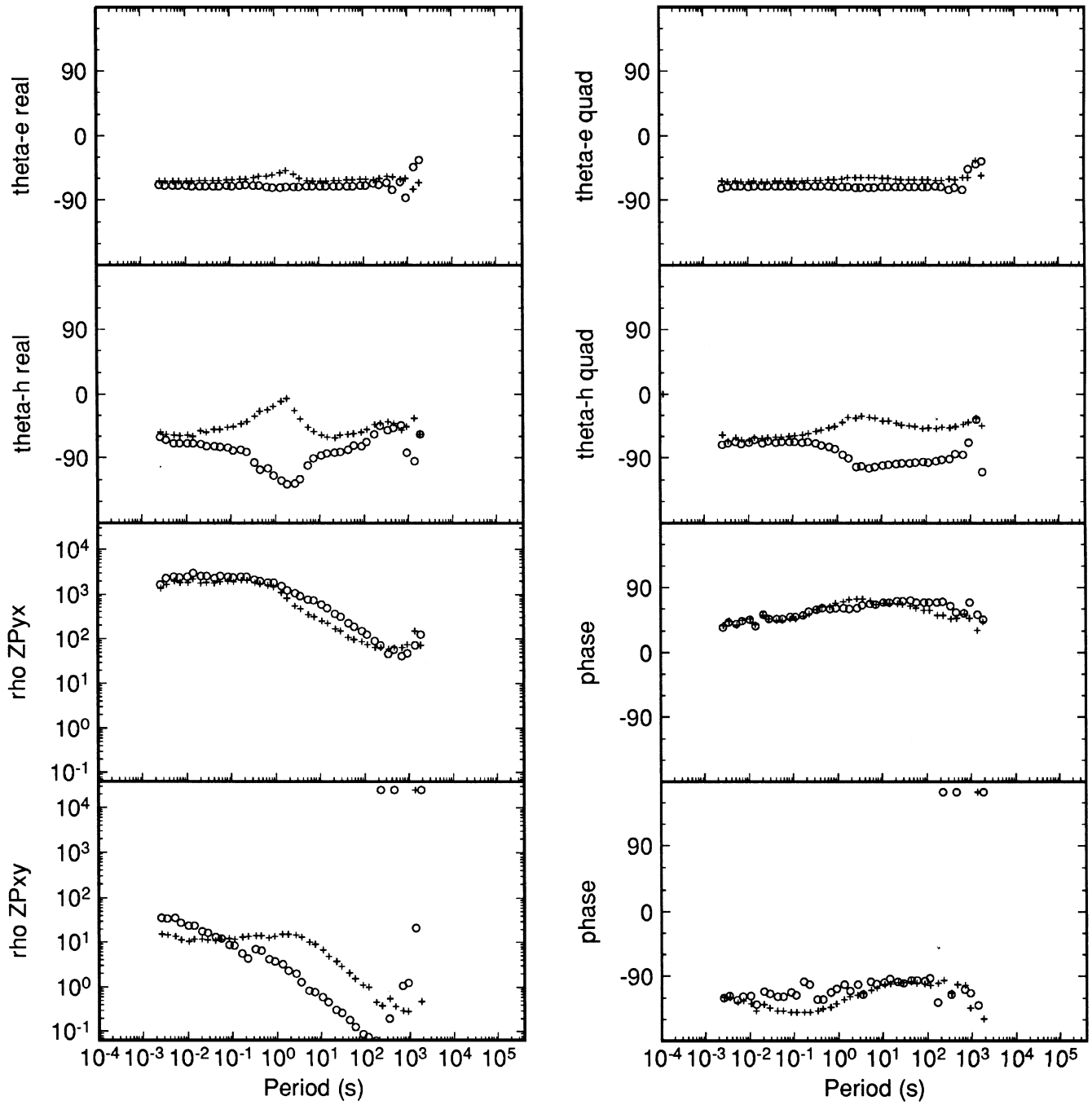

FIG. 4. Superimposed plots for decomposition parameters of LIT007 (circles) and LIT008 (crosses).

ACKNOWLEDGMENTS

I thank Alan Jones for circulating the BC87 data, and for initiating and leading the MTDIW workshops of 1992 and 1994; I thank others at the meetings for their discussion. Key elements of the results presented in this paper were seen first in the Mohr diagram plots; for much insight in interpreting these, I thank Win Means. The comments of Associate Editors and referees have added greatly to this paper. The BC87 data are part of Canadian Lithoprobe.

REFERENCES

Chave, A. D., and Jones, A. G., 1997, Electric and magnetic field galvanic distortion decomposition of BC87 data: J. Geomag. Geoelectr., **49**, 767–789.

Groom, R. W., Kurtz, R. D., Jones, A. G., and Boerner, D. E., 1993, A quantitative methodology to extract regional magnetotelluric impedances and determine the dimension of the conductivity structure: Geophys. J. Internat., **115**, 1095–1118.

Ingham, M. R., Jones, A. G., and Honkura, Y., 1993, Eds., Electromagnetic induction in the Earth: J. Geomag. Geoelectr., **45**, 703–1150.

Jones, A. G., 1993, The BC87 dataset: tectonic setting, previous EM results, and recorded MT data: J. Geomag. Geoelectr., **45**,

1089–1105.
Jones, A. G., and Groom, R. W., 1993, Strike-angle determination from the magnetotelluric impedance tensor in the presence of noise and local distortion: rotate at your peril!: Geophys. J. Internat., **113**, 524–534.
Jones, A. G., Kurtz, R. D., Oldenburg, D. W., Boerner, D. E., and Ellis, R., 1988, Magnetotelluric observations along the LITHOPROBE southeastern Canadian cordilleran transect: Geophys. Res. Lett., **15**, 677–680.
Lilley, F. E. M., 1998, Magnetotelluric tensor decomposition: 1. Theory for a basic procedure: Geophysics, **63**, 1885–1897.
Means, W. D., 1992. How to do anything with mohr circles: A short course about tensors for structural geologists: State Univ. of New York at Albany.

APPENDIX A

HOW TO SKETCH A Z'_{xy_r} VERSUS Z'_{xx_r} MOHR DIAGRAM FOR MT DATA (ADAPTED FROM MEANS, 1992)

A simple way to sketch a Mohr diagram for a known impedance tensor is as follows. On cartesian axes with Z'_{xy_r} horizontally to the right and Z'_{xx_r} upwards, plot the point (Z_{xy_r}, Z_{xx_r}) using values from the real part of the tensor. Then, plot the point ($-Z_{yx_r}$, Z_{yy_r}), and draw the circle for which these two points form a diameter. Join the center of the circle to the origin: the angle this line makes with the horizontal axis is the skew or twist of the real part of the tensor [it will be γ_r, as γ_r is defined in equation (2) above]. Join the center of the circle to the first point plotted: rotation of this radial arm by angle $2\theta'$ anticlockwise takes one around the circle to the values of Z'_{xy_r} and Z'_{xx_r}, which the tensor would have upon rotation of the measuring axes by angle θ' clockwise. A similar procedure may be carried out for the quadrature parts of the tensor.

An example is shown in Figure A-1 for the matrix

$$\begin{bmatrix} 3 & 7 \\ -4 & -1 \end{bmatrix}.$$

The point (7, 3) is plotted first, followed by the point (4, −1). These two points define a diameter for the circle, and thus its central point. A line is drawn, joining the center to the origin of axes. A radial arm is then drawn from the center to the first point, (7, 3).

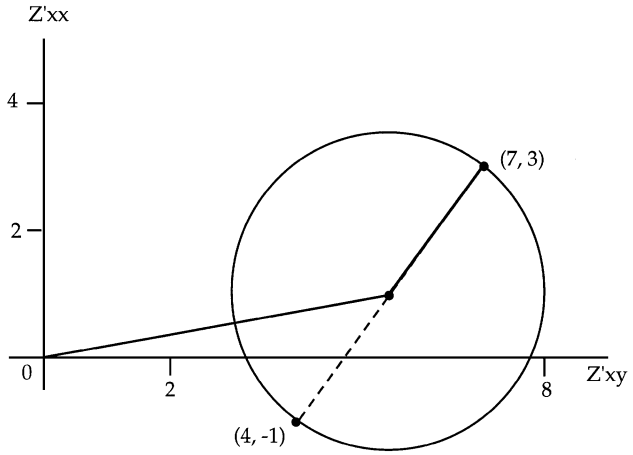

FIG. A-1. Procedure for sketching a Mohr diagram for the matrix $\begin{bmatrix} 3 & 7 \\ -4 & -1 \end{bmatrix}$